

Intertidal finger bars at El Puntal, Bay of Santander, Spain

E. Pellón et al.

This discussion paper is/has been under review for the journal Earth Surface Dynamics (ESurFD). Please refer to the corresponding final paper in ESurFD if available.

Intertidal finger bars at El Puntal, Bay of Santander, Spain: observation and forcing analysis

E. Pellón, R. Garnier, and R. Medina

Environmental Hydraulics Institute (IH Cantabria), Universidad de Cantabria, Santander, Spain

Received: 15 October 2013 – Accepted: 26 October 2013 – Published: 13 November 2013

Correspondence to: E. Pellón (pellone@unican.es) and R. Garnier (garnier@unican.es)

Published by Copernicus Publications on behalf of the European Geosciences Union.

Title Page

Abstract

Introduction

Conclusions

References

Tables

Figures



Back

Close

Full Screen / Esc

Printer-friendly Version

Interactive Discussion



Abstract

A system of 15 small-scale finger bars has been observed, by using video imagery, between 23 June 2008 and 2 June 2010. The bar system is located in the intertidal zone of the swell-protected beaches of El Puntal Spit, in the Bay of Santander (Northern coast of Spain). It appears on a planar beach (slope = 1.5%) with fine uniform sand ($D_{50} = 0.27$ mm) and extends 600 m alongshore. The cross-shore span of the bars is determined by the tidal horizontal excursion (between 70 and 130 m). They have an oblique orientation with respect to the low-tide shoreline being up-current oriented with respect to the ebb-flow (mean angle of 26° from the shore normal). Their mean wavelength is 26 m and their amplitude varies between 10 and 20 cm. The full system slowly migrates to the east (opposite to the ebb-flow) with a mean speed of 0.06 m day^{-1} , a maximum speed in winter (up to 0.15 m day^{-1}) and a minimum speed in summer. An episode of merging has been identified as bars with larger wavelength seem to migrate slower than shorter bars. Several forcings can act on the bar dynamics being the wind, blowing predominantly from the west, the main candidate to explain the eastward migration of the system. In particular, the wind can generate waves of up to 20 cm (root-mean-squared wave height) over a fetch that can reach 4.5 km at high tide. The astronomical tide seems to be important in the bar dynamics, as the tidal range conditions the mean (daily) fetch and also the time of exposure of the bars to the marine dynamics. Furthermore, the river discharges could act as input of suspended sediment in the bar system and play a role in the bar dynamics.

1 Introduction

Transverse bars are morphological features attached to the shore that appear with a noticeable rhythmicity along the coast of sandy beaches. They have been identified in many types of environments and have been observed with a wide range of characteristics so that a classification of the existing bar systems is necessary. This is not

ESURFD

1, 673–710, 2013

Intertidal finger bars at El Puntal, Bay of Santander, Spain

E. Pellón et al.

Title Page

Abstract

Introduction

Conclusions

References

Tables

Figures

◀

▶

◀

▶

Back

Close

Full Screen / Esc

Printer-friendly Version

Interactive Discussion



straightforward as these features can be classified with regard to many criteria such as their geometry (length scale, orientation with respect to the shoreline), their dynamics (formation time, migration), or the hydro-morphological environment they pertain. Alternatively, this can be made based on the physical processes governing their formation and their dynamics, although this is sometimes not well understood.

The most documented and observed transverse bar types are probably the “TBR” (“Transverse Bar and Rip”) described by Wright and Short (1984) printing a cusped signature on the shoreline called magacusp (Thornton et al., 2007). They sometimes appear with an oblique orientation with respect to the shoreline (Lafon et al., 2002; Castelle et al., 2007). The TBR are typically linked to outer morphological patterns, precisely, they form due to the onshore migration of a crescentic bar (Ranasinghe et al., 2004; Garnier et al., 2008). They are generally found on open coasts in intermediate wave-dominated beaches, with wavelength (distance between two bars) of 100–500 m, and are associated with the presence of rip currents flowing offshore between two bars. Remarkably, the recent study of Goodfellow and Stephenson (2005) shows that these systems can appear, at smaller scale, in lower energy environment (40 km limited fetch).

Here we will focus on “(transverse) finger bars” that differ from the TBR as they do not emerge from off-shore bathymetric features but they are assumed to form “alone”. Moreover, they are not necessarily associated with rip currents. Regarding their geometry, the main difference with the TBR is that they are long crested, i.e., their cross-shore extent is generally larger than their wavelength. We identify three types of finger bars (Table 1).

1. The first type of finger bars has been identified by Niedoroda and Tanner (1970). We will refer to them as “large scale finger bars” because of their large cross-shore span (~ 1 km). Their wavelength is ~ 100 m and they appear in low energy environments (mean wave height < 0.5 m) on very wide (~ 1 km) beaches with a gentle slope (0.002). They are oriented almost perpendicularly to the shore or

Intertidal finger bars at El Puntal, Bay of Santander, Spain

E. Pellón et al.

Title Page

Abstract

Introduction

Conclusions

References

Tables

Figures



Back

Close

Full Screen / Esc

Printer-friendly Version

Interactive Discussion



with a slight obliquity, in both micro- and macro-tidal environments (Gelfenbaum and Brooks, 2003; Levoy et al., 2013).

2. Although finger bars are often associated with very low wave energy (Wijnberg and Kroon, 2002) a second type of finger bars can be observed in intermediate morphological beach states (Konicki and Holman, 2000; Ribas and Kroon, 2007). They coexist, at a smaller wavelength (50–100 m), with other rhythmic morphologies present in the surf-zone, such as with TBR and with crescentic bars. One of the particularities of these “finger bars of intermediate beaches” is that they have an oblique up-current orientation with respect to the mean alongshore current (Ribas et al., 2012).
3. Finally, a third type of finger bars, the “small scale finger bars” appear for very low wave energy in very fetch limited environment (fetch < 10 km), with wave length of ~ 10 m and a cross-shore span (10–100 m) that depends of the horizontal tidal excursion (Bruner and Smosna, 1989; Garnier et al., 2012). These bars are not strictly normal to the shore (Falqués, 1989; Nordstrom and Jackson, 2012) but seem to be down-current oriented with respect to the sand transport (Bruner and Smosna, 1989) that is opposite to the finger bars of intermediate beaches.

The processes of generation and evolution of finger bars are probably different depending on their type, and, particularly, depending on their orientation. Finger bar systems generally migrate in the direction of the sediment transport, but this is not always identified, possibly due to the lack of field data. For instance, the theoretical modelling studies of Ribas et al. (2003) and of Garnier et al. (2006) have shown different mechanisms to explain the dynamics of up- and down-current oriented bars by considering forcing due to waves. This has been successfully applied to the finger bars of intermediate beach by Ribas et al. (2012) based on continuous observations obtained from video imagery. However, the dynamics of finger bars appearing in low energy environment is poorly understood, especially concerning the small scale finger bars as (1) the forcing acting on their dynamics is difficult to determine as, in very limited fetch envi-

Intertidal finger bars at El Puntal, Bay of Santander, Spain

E. Pellón et al.

Title Page

Abstract

Introduction

Conclusions

References

Tables

Figures



Back

Close

Full Screen / Esc

Printer-friendly Version

Interactive Discussion



Intertidal finger bars at El Puntal, Bay of Santander, Spain

E. Pellón et al.

Title Page

Abstract

Introduction

Conclusions

References

Tables

Figures

◀

▶

◀

▶

Back

Close

Full Screen / Esc

Printer-friendly Version

Interactive Discussion



ronment, wind, waves and tidal current, can act with similar intensities, and (2) there is no continuous survey of such systems. Some recent studies have performed the monitoring of large scale finger bars allowing them to detect mean velocities of less than 2 m month^{-1} (Gelfenbaum and Brooks, 2003; Levoy et al., 2013) and maximum velocities of 1 m day^{-1} (Levoy et al., 2013). Concerning small scale finger bars, only the preliminary study of Garnier et al. (2012) gave information on the dynamics of such systems, but, the migration speeds detected are overestimated due to strong noise in the data.

The objective of this contribution is to get insight into the dynamics of small scale transverse bars by performing a continuous survey of finger bars detected in the Bay of Santander, Spain, and by analysing the possible forcing that can act in their dynamics. These finger bars are located in the intertidal zone and the survey is performed by using video images at low tide. Section 2 presents the field site and the dataset obtained by video imagery. Section 3 describes the characteristics and the dynamics of the bar system. Section 4 reports the forcing analysis based essentially on wind data. Section 5 is the conclusion.

2 Field site and video imagery

2.1 Study site

El Puntal spit is part of the natural closure of the Bay of Santander (Fig. 1). This bay is one of the largest estuaries of the northern coast of Spain (Cantabrian Sea). The closure of the bay is composed by two natural formations, the Magdalena peninsula at the north-west, and El Puntal spit at the north-east. This spit is a sand accumulation which extends from east to west along approximately 2.5 km. Historically, more than 50 % of the surface of this bay has been filled in, reducing the tidal prism and changing the morphological equilibrium of El Puntal (Losada et al., 1991) which tends to extend

up-current oriented with respect to the ebb-flow. The bars are more regularly spaced and parallel in the eastern half of the area, the western bars are more irregular, with slight changes in direction and bifurcations (Fig. 1d).

The intertidal beach where the bars appear is planar with a constant slope of approximately 1.5%. The offshore boundary of the bars is delimited by a steep slope that ends in the subtidal channel. Sediment sampling has shown the same grain size on bars and troughs with $D_{50} = 0.27$ mm.

2.2 Video imagery

In the last decades, video monitoring systems are increasingly used to study the shoreline around the world (Holman et al., 1993). To extract geometric data of the bar system, the images of the Horus video imagery system were used (www.horusvideo.com). This system is composed by 4 cameras located at the roof of the Hotel Real (Fig. 3a), at 91 m above the mean sea level and 1.5 km from the study area. This system was set in 2008 and takes images each 10 min. In the present study only camera 2 has been used (Fig. 3b). The pixel resolution on the study area is variable on the alongshore direction, with values from 4.5 m pixel^{-1} to 6.6 m pixel^{-1} . On the cross-shore direction the resolution is around 0.5 m pixel^{-1} . One daily image of the bar system has been selected at low tide between 23 June 2008 and 2 June 2010, which is the longest period found without long interruptions in the image database. All the interruptions were of less than 6 consecutive days and were due to technical problems (27 days) and bad meteorological conditions (fog 18 days, strong wind 3 days and bad sharpness 85 days). The geometry of the bars was extracted on 577 days, which is an 81% of the time.

Each bar has been digitized manually by selecting 3 points on each: at the upper part of the beach, at the middle of the bar and at the offshore end of the bar (Fig. 4). It was checked that 3 points per bar is enough to describe their geometry. Finally, the digitized data was rectified by means of 7 Geographic Control Points (GCP), obtaining the geographic coordinates of each digitized point.

Intertidal finger bars at El Puntal, Bay of Santander, Spain

E. Pellón et al.

Title Page

Abstract

Introduction

Conclusions

References

Tables

Figures



Back

Close

Full Screen / Esc

Printer-friendly Version

Interactive Discussion



Intertidal finger bars at El Puntal, Bay of Santander, Spain

E. Pellón et al.

Title Page

Abstract

Introduction

Conclusions

References

Tables

Figures



Back

Close

Full Screen / Esc

Printer-friendly Version

Interactive Discussion



The data processed by Garnier et al. (2012) has been re-analysed in order to correct an apparent periodic movement due to sun shadows in the bars. The amplitude of this periodic movement is of the order of the pixel resolution and it has been found that its period is related with the capture times. Furthermore, this apparent movement seems to be a systematic error linked to the different sun positions at low tide during the fortnightly cycle of neap-spring tides, which causes different shadows by the bars and different light reflections in the wet areas.

All the measurements of the bar geometry are referenced to the y axis that is parallel to the shoreline at low tide (113° from the north, Fig. 4). The bar wavelength and the migration velocities are measured with respect to the y axis. The angle of the bars is measured from the x axis. During a tidal cycle, the mean shoreline position is approximately parallel to the y axis, except at the highest levels of spring tides. To better characterize the behaviour of the finger bars each bar has been characterised by 4 positions along the y_1 – y_4 axes (parallel to the y axis) scattered trough the intertidal zone, at different levels (see Fig. 4). Each line represents one level along the whole study area (Fig. 5c) and all these lines together are representative of the whole width of the bars.

3 Bar characteristics and dynamics

3.1 Bathymetry reconstruction

The Horus system captures one image of the study area every 10 min. This means that the path of the shoreline can be observed along the tidal cycle with high frequency. To obtain information about the 3-D geometry of the finger bar system a reconstruction of the intertidal bathymetry of the study area has been performed (Fig. 5a). This must be done at one day with good meteorological conditions and enough sharpness in all the images during the rising tide. This tide should have the highest range possible, allowing to extract data of a larger intertidal region, taking into account that it has to

Intertidal finger bars at El Puntal, Bay of Santander, Spain

E. Pellón et al.

Title Page

Abstract

Introduction

Conclusions

References

Tables

Figures



Back

Close

Full Screen / Esc

Printer-friendly Version

Interactive Discussion



occur completely during the day light. After this, the shoreline is digitized and rectified on each image. To obtain the bathymetry we assume that the sea level measured at the tide gauge of Santander (at less than 2 km) is the same as the level of the shoreline in the study area. The level with respect to the zero of the harbour of Santander (Z) is associated to each rectified shoreline, obtaining the intertidal bathymetry of Fig. 5a.

Cross-shore profiles of this bathymetry (Fig. 5c) show that the bars only appear on the region of the intertidal beach profile which has constant slope of 1.5 %. The extraction of longitudinal profiles from this bathymetry allows us to measure the amplitude of the bars, which oscillates between 10 and 20 cm. These profiles also show the asymmetry of the bars (Fig. 5b) with steeper slopes on the lee sides (relative to the migration direction), in agreement with previous studies (Gelfenbaum and Brooks, 2003).

3.2 Bar dynamics

During the 2 yr study period the position and geometry of 15 bars have been daily digitized. Figure 6 shows the position of the bar system along the y_3 axis. The bar system is persistent along the time, appearing in all the observed images with similar geometric characteristics and extending along the same area, but the entire system slowly migrates to the east. As a result of the eastward migration a new bar becomes visible at the west end of the study area (Bar 1, Fig. 6). Although aerial images and the migration of the system suggest that the bars are formed at the west of the study area, the formation area is not included in the present results as it is hidden by the dune (Fig. 5a). At the east end of the area, the last bar decays and slowly disappears. Remarkably, for the whole study period, an episode of merging of two bars into one has been detected on 28 March 2009 (Fig. 6).

3.2.1 Mean motion

The digitized and rectified data allow the daily measurement of the bar wavelength. For each bar, the wavelength has been averaged along the complete study period (Fig. 7).

Intertidal finger bars at El Puntal, Bay of Santander, Spain

E. Pellón et al.

Title Page

Abstract

Introduction

Conclusions

References

Tables

Figures

◀

▶

◀

▶

Back

Close

Full Screen / Esc

Printer-friendly Version

Interactive Discussion



have been decomposed in segments of variable length. The segment length has been set in order to minimise the error between the piecewise signal and the measured positions. For each signal, the number of segments has been found such that the mean length corresponds to 70 days (Fig. 6). For each segment, we can therefore obtain the approximate bar migration V_k , associated to the time interval T_k .

Considering that, at a time t , N segments are obtained (for all the bars of the system), the migration velocity of the bar system V_m (Fig. 8) is computed as:

$$V_m(t) = \sum_{i=1}^{N(t)} \frac{\hat{V}_i(t)}{N(t)}, \text{ where } \hat{V}_i(t) = \begin{cases} V_k, & \text{if } t \in T_k \\ 0, & \text{elsewise} \end{cases} \quad (1)$$

The migration velocity of the bar system is not constant along the time. It shows maximum velocities during winter. The maximum speeds, of about 0.15 m day^{-1} , were reached during the first winter studied (2009), while during the second winter (2010) the maximum speeds are lower than 0.1 m day^{-1} . During summer the system migration is slower, with negative speeds for summer 2008, and velocities lower than 0.01 m day^{-1} for summer 2009. The negative velocities (i.e. migration to the west) found in summer 2008 can be due to limitations in the computation of V_m that can occur for several reasons. Firstly an error in the bar detection or an error in the interpolation (piecewise approximation) can result in an erroneous apparent bar motion. Secondly, this is not observed for all the bars and for all the positions (Fig. 6), the negative velocities observed can represent, instead of a westward migration, a change in shape of some bars.

4 Forcing analysis

4.1 Forcing candidates

The migration to the east of the bar system indicates a dominant forcing coming from the west. The wind data has been extracted from the SeaWind (Menéndez et al., 2011)

Intertidal finger bars at El Puntal, Bay of Santander, Spain

E. Pellón et al.

Title Page

Abstract

Introduction

Conclusions

References

Tables

Figures

⏪

⏩

◀

▶

Back

Close

Full Screen / Esc

Printer-friendly Version

Interactive Discussion



model (Booij et al., 1999). In the computations, changes in tidal level affecting the fetch have been included. The time series of the wind-waves have been obtained with an interpolation technique based on radial basis functions (RBF), a scheme which is very convenient for scattered and multivariate data (Camus et al., 2011). Results of the root-mean-square (rms) wave height H_{rms} of the waves entering in the bar system are displayed in Fig. 9b (wave rose) and in Fig. 9f (time series of the daily averaged rms wave height). The waves arrive from the west-south-west and south-west during the 65% of the time, with mean (rms) wave height of 5 cm and period of 1.5 s. During the westward windstorms the waves can reach 0.2 m from the west-south-west, with period of 3 s. The other 35% of the time the waves come from the east-south-east, with wave height lower than 7 cm and period below 1.7 s. The mean wave height from this sector is less than 2 cm with 1.2 s of period.

Hydrodynamic studies of the Santander Bay have highlighted the effect of the water discharge produced by the Miera River (at the east of the study area) in the annual mean current magnitude in the Bay (Bidegain et al., 2013). Time series of the daily averaged river flow rate are shown in Fig. 9e. Bidegain et al. (2013) have shown that, although the effect of the river is strong in the channel (ebb-oriented flow), the current produced close to the bar system is weak. However, the river discharge can play a role in the bar dynamics as it is linked to a strong sediment supply, that can act as an input of suspended sediment to the bar system.

4.2 Wind and wind-waves

The previous studies on transverse bars, where the waves appear clearly to be the main forcing, usually use different indicators to relate the dynamics of the bars with the incident forcing (e.g. Ribas and Kroon, 2007; Castelle et al., 2007; Price and Ruessink, 2011).

Castelle et al. (2007) and Price and Ruessink (2011) use the off-shore wave power (P , also called wave energy flux) and the alongshore wave power (P_y) defined as:

$$P = \frac{\rho g^2}{32\pi} H_{\text{rms}}^2 T_p, \text{ and } P_y = P \sin \theta \cos \theta \quad (2)$$

where ρ is the water density ($\rho = 1025 \text{ kg m}^{-3}$), g the gravitational acceleration ($g = 9.81 \text{ ms}^{-2}$), T_p is the peak wave period and θ is the offshore wave angle (from the shore-normal).

Ribas and Kroon (2007) use the alongshore component of the wave radiation stress as an indicator of the alongshore current magnitude defined as (Longuet-Higgins and Stewart, 1964):

$$S_{xy} = \frac{\rho g}{16} H_{\text{rms}}^2 \sin \theta \cos \theta \quad (3)$$

The time series of the daily averaging, and the seasonal averaging of these variables are plotted in Fig. 10a and b, and Fig. 11a and b, respectively. The results show that the largest migration velocities occurring during autumn, winter and early spring corresponds to the largest values of P_y and of S_{xy} . However, nor the daily averaged signals nor the seasonal averaged quantities can explain why the bars migrate faster in winter 2009 than in winter 2010.

Compared with previous studies in wave-dominated environment, there is a difference of about two orders of magnitude in these variables. While Ribas and Kroon (2007) observed the same difference concerning the migration speed of the bars, the bar system observed by Castelle et al. (2007) migrates slowly, relatively. This is probably due to the different mechanisms governing the dynamics of TBR (Castelle et al., 2007) and finger bars (Ribas and Kroon, 2007).

The effect of the local wind is now analysed by computing the alongshore component of the wind stress (Fig. 10c) defined as:

$$T_y = -\rho C_f W^2 \cos \theta_w \quad (4)$$

Intertidal finger bars at El Puntal, Bay of Santander, Spain

E. Pellón et al.

Title Page

Abstract

Introduction

Conclusions

References

Tables

Figures



Back

Close

Full Screen / Esc

Printer-friendly Version

Interactive Discussion



where C_f is the friction coefficient, adimensional and equal to 1.2×10^{-6} , W is the wind speed module and θ_w is the incoming wind angle (from the shore-normal).

In order to compare the relative effect of the wind and of the wind waves we define the alongshore wave stress $S_y = S_{xy}/X_b$ (Fig. 11c), with X_b , the surf-zone width computed with $X_b = H_{rms}/(\gamma_b \times \beta)$:

$$S_y = \frac{\rho g H_{rms}}{16 \beta \gamma_b} \sin \theta \cos \theta \quad (5)$$

where γ_b is the breaking coefficient for irregular waves ($\gamma_b = 0.42$, Thornton and Guza, 1983) and β is the beach slope ($\beta = 0.015$).

The comparison of Fig. 11c and d shows that both forcings have the same order of magnitude and can therefore play a role in the bar dynamics, although S_y is twice larger than T_y . The seasonal analysis of the wind stress is the only one that shows higher energetic conditions in winter 2009 than in winter 2010, according to the results of the migration speed.

4.3 Sediment transport evaluation

The relationship between the bar migration and the alongshore component of the sediment transport is here investigated. Because of the uncertainties in the sediment transport formulations, two different formulas will be used, based on the previous theoretical study of Garnier et al. (2006). We will perform the analysis by considering (1) the simplest sediment transport formulation by assuming that the alongshore component of the sediment transport is proportional to the depth-averaged mean fluid velocity and (2) a more sophisticated formulation based on the Soulsby and Van Rijn formula (Soulsby, 1997). These two formulations have been used in modelling studies to explain the formation of different kinds of transverse bars (Ribas et al., 2003; Garnier et al., 2006). Here, we assume that the general formulation of the alongshore component of the

Intertidal finger bars at El Puntal, Bay of Santander, Spain

E. Pellón et al.

Title Page

Abstract

Introduction

Conclusions

References

Tables

Figures

◀

▶

◀

▶

Back

Close

Full Screen / Esc

Printer-friendly Version

Interactive Discussion



sediment transport is given by:

$$q = \alpha (V_{\text{wave}} + V_{\text{wind}}) \quad (6)$$

where α is the sediment stirring function, V_{wave} is the alongshore component of the wave and depth-averaged current driven by the wind-waves, and V_{wind} is the alongshore component of the depth-averaged current driven by the local wind.

In order to analyse the correlation between q and the bar velocities, we will integrate the sediment transport over the time interval T_k , for each segment that characterise the bar movement (Sect. 3.2.2).

4.3.1 Constant stirring

The first formulation is based on a constant stirring function. The correlation can be examined directly by using the alongshore current magnitude. The first part of the analysis can be done by analysing V_{wind} and V_{wave} , by separately, to distinguish the respective contributions of the wind and the wind-waves.

The alongshore current generated by the wind is computed by assuming the alongshore momentum balance between the wind stress and the bottom friction in case of a quadratic friction law:

$$V_{\text{wind}} = \pm \left| \frac{T_y}{\rho c_d} \right|^{0.5} \quad (7)$$

with c_d , the hydrodynamic drag coefficient set as $c_d = 0.005$.

The alongshore current generated by the wind-waves is approximated from the formula presented by Komar and Inman (1970). It reads:

$$V_{\text{wave}} = 1.17(gH_{\text{rms}})^{0.5} \sin \theta_b \cos \theta_b \quad (8)$$

where θ_b is the wave angle at breaking. It has been evaluated at the breaking depth defined as H_{rms}/γ_b ($\gamma_b = 0.42$) from the incident wave angle computed with the SWAN model (Sect. 4.1) by using the Snell law and the dispersion relationship.

Intertidal finger bars at El Puntal, Bay of Santander, Spain

E. Pellón et al.

Title Page

Abstract

Introduction

Conclusions

References

Tables

Figures

◀

▶

◀

▶

Back

Close

Full Screen / Esc

Printer-friendly Version

Interactive Discussion



Intertidal finger bars at El Puntal, Bay of Santander, Spain

E. Pellón et al.

Title Page

Abstract

Introduction

Conclusions

References

Tables

Figures

◀

▶

◀

▶

Back

Close

Full Screen / Esc

Printer-friendly Version

Interactive Discussion



The seasonal variations of V_{wind} and V_{waves} (Fig. 12a and c) show similar tendencies. The minimum velocities are obtained in summer and the mean velocities observed in winter 2009 are smaller than in winter 2010 (contrarily to the migration speed of the bar system). The current velocities driven by the wind-waves are more than two times larger than the wind driven velocities.

Results of the correlation between these current velocities shows similar results (Fig. 12b and d, Table 2), with correlation coefficient of 0.46 and 0.49, with the best result obtained by considering only the wind driven current, and by considering the total transport (Eq. 6).

4.3.2 Soulsby and Van Rijn (SVR) formula

The tests performed with the simple formula do not show the clear influence of wind-waves in our fetch limited environment, maybe because they do not consider the effect of sediment stirring by waves, nor the critical velocity necessary to move sediment.

Here, we will use a more realistic transport formula based on the Soulsby and Van Rijn formula (Soulsby, 1997). We approximate the stirring function as:

$$\alpha_{\text{SVR}} = \begin{cases} A_S (U_{\text{eq}} - U_{\text{crit}})^{2.4} & \text{if } U_{\text{eq}} > U_{\text{crit}} \\ 0 & \text{otherwise} \end{cases} \quad (9)$$

where A_S is a coefficient that represents the suspended load and the bed load transport and U_{crit} is the critical velocity above which the sediment can be transported. They depend essentially on the sediment characteristics and on the water depth (for more details see Soulsby, 1997; Garnier et al., 2006). The equivalent stirring velocity is defined as:

$$U_{\text{eq}} = \left(U_{\text{wind}}^2 + V_{\text{wave}}^2 + \frac{0.018}{C_d} U_b^2 \right)^{0.5} \quad (10)$$

where U_{wind} is the velocity amplitude of the current generated by the wind, U_b is the wave orbital velocity amplitude at the bottom (computed at wave breaking) and C_d is the morphodynamic drag coefficient computed with the formula of Soulsby (1997).

Tests performed by neglected the effect of waves show very poor correlation as the wind driven current is not enough to transport the sediment even at very small depth (where U_{crit} is the smallest). As the previous result suggested, most of the stirring is enhanced by the wind-waves.

Figure 12e shows that the sediment transport is larger in winter 2009 than in winter 2010, in agreement with the tendency of the migration velocity. Furthermore, it shows a weaker transport in spring 2009 than in spring 2010 corresponding to a smaller migration velocity. This explains why the correlation (Fig. 12f, Table 2) is better than the one obtained with a constant wave stirring. Here, the correlation coefficient is 0.58.

Although the tidal level variation has been considered to compute the wind-wave time series, the effect of additional stirring that can appear during spring tides and the difference in active time (time while the bars are impacted by the marine dynamics) depending on the tidal range, have not been included in the previous formula. Inclusion of an additional stirring in Eq. (10) due to tide does not improve the results. However, multiplying the Eq. (9) by a correction factor $\alpha_t = \min(\text{TR})/\text{TR}$, where TR is the tidal range gives a correlation of 0.60 (Fig. 12g and h, Table 2). This simply simulates the fact that maximum transport occurs during neap tide as the bar system is active during a larger period.

Figure 9e shows the flow rate of Miera river. This flow rate is bigger during winter 2009 than winter 2010, so the faster migration speed of the bars during this period could be influenced by the river discharge, maybe because it is a source of sediment. However, tests performed by including additional sediment stirring due to the river flow do not show improvement of the results.

None of the models used here manages to predict the negative (westward) migration reported during summer 2008. This supports the possible error in the velocity computation previously mentioned.

Intertidal finger bars at El Puntal, Bay of Santander, Spain

E. Pellón et al.

Title Page

Abstract

Introduction

Conclusions

References

Tables

Figures



Back

Close

Full Screen / Esc

Printer-friendly Version

Interactive Discussion



5 Conclusions

A small-scale finger bar system has been identified on the intertidal zone of the swell-protected beach of El Puntal Spit in the Bay of Santander (northern coast of Spain). The beach is characterised by a constant slope of 1.5% and by uniform sand with $D_{50} = 0.27$ mm. This system appears on the flat intertidal region, which extends over 600 m on the alongshore direction and between 70 m and 130 m on the cross-shore direction (the cross-shore span is determined by the tidal horizontal excursion).

A system of 15 bars has been observed by using the Horus video imagery system during 2 yr (between 23 June 2008 and 2 June 2010). The bar system has been digitized from daily images at low tide. The data set is almost continuous, with good quality data the 81% of the time and a maximum continuous period of time without data of 6 days.

The geometric characteristics of the system are almost constant along the time. The mean wavelength of the bar system is 26 m and the bar amplitude is between 10 and 20 cm. Moreover, the bars have an oblique orientation with respect to the low-tide shoreline, with a mean angle of 26° to the east from the shore-normal. We noticed differences in the geometry along the domain: the western bars (first half) are more irregular and have smaller wavelength than the eastern bars (second half).

The full system slowly migrates to the east (against the ebb-flow) with a mean speed of 6 cm day^{-1} that varies between bars. In general the larger is the wavelength the slower is the migration velocity, in agreement with previous studies on transverse bars. Remarkably, an episode of merging of two bars has been observed on 28 March 2009: the bar with the smallest wavelength is faster and merges with the next bar. As bars migrate to the east, they form at the west and decay at the east.

A detailed analysis of the bar motion, from a piecewise regression of the bar positions, have shown that bars migrates faster in winter and slower in summer, with maximum velocities obtained in winter 2009 (0.15 m day^{-1}). Some negative velocities

ESURFD

1, 673–710, 2013

Intertidal finger bars at El Puntal, Bay of Santander, Spain

E. Pellón et al.

Title Page

Abstract

Introduction

Conclusions

References

Tables

Figures

◀

▶

◀

▶

Back

Close

Full Screen / Esc

Printer-friendly Version

Interactive Discussion



(migration to the west) have been computed (during summer 2008) but this result could be not realistic.

Several forcings can act on the bar dynamics being the wind, blowing predominantly from the west, the main candidate to explain the eastward migration of the system. Off-shore of the bar system, the mean (annual) flow is ebb-oriented (to the west), because of the Miera river discharge and of the astronomical tide, however, in the intertidal zone their effect on the mean flow vanishes. There, wind and wind-waves generated over a fetch of up to 4.5 km at high tide, seem to determine the direction of the alongshore transport.

Although residual tidal current is weak, the tide seems to be important in the bar dynamics as the tidal range conditions the mean (daily) fetch and also the time of exposure of the bars to the marine dynamics. Furthermore, the river discharge could act as input of suspended sediment in the bar system and play a role in the bar dynamics.

The correlation between the bar migration and the alongshore component of the sediment transport has been analyzed by using different transport formulas. Best results (correlation coefficient of 0.6) has been obtained by considering the Soulsby and Van Rijn formula including sediment stirring by the locally generated waves and by including a correction factor to simulate that the active time depends on the tidal range.

Finally, the bar system is persistent and no formation and no destruction events of the entire system have been observed. Further studies are necessary to understand the formation processes and the full dynamics of these small-scale finger bars. In-situ measurements of the hydrodynamics and sediment concentrations and numerical morphological modelling are essential to deepen on the analysis. The bar system here has an oblique down-current orientation with respect to the migration direction and has similar characteristics and dynamics than the system described by previous theoretical (modelling) studies that consider the forcing due to waves only. However, in our estuarine environment, the dynamics is more complex as different forcings act with the same order of magnitude.

Intertidal finger bars at El Puntal, Bay of Santander, Spain

E. Pellón et al.

Title Page

Abstract Introduction

Conclusions References

Tables Figures

◀ ▶

◀ ▶

Back Close

Full Screen / Esc

Printer-friendly Version

Interactive Discussion



Discussion Paper | Discussion Paper | Discussion Paper | Discussion Paper | Discussion Paper

Acknowledgements. The authors thank Puertos del Estado (Spanish Government) for providing tide-gauge data. The work of R. Garnier is supported by the Spanish Government through the “Juan de la Cierva” program. This research is part of the ANIMO (BIA2012-36822) project which is funded by the Spanish government.

5 References

- Bárcena, J. F., García, A., García, J., Álvarez, C., and Revilla, J. A.: Surface analysis of free surface and velocity to changes in river flow and tidal amplitude on a shallow mesotidal estuary: an application in Suances Estuary (Northern Spain), *J. Hydrol.*, 14, 301–318, 2012.
- 10 Bidegain, G., Bárcena, J. F., García, A., and Juanes, J. A.: LARVAHS: predicting clam larval dispersal and recruitment using habitat suitability-based particle tracking mode, *Ecol. Model.*, 268, 78–92, 2013.
- Booij, N., Ris, R. C., and Holthuijsen, L. H.: A third-generation wave model for coastal regions, Part I, Model description and validation, *J. Geophys. Res.*, 104, 7649–7666, 1999.
- Bruner, K. R. and Smosna, R. A.: The movement and stabilization of beach sand on transverse bars, Assateague Island, Virginia, *J. Coastal Res.*, 5, 593–601, 1989.
- 15 Camus, P., Méndez, F. J., and Medina, R.: A hybrid efficient method to downscale wave climate to coastal areas, *Coast. Eng.* 58, 851–862, 2011.
- Castelle, B., Bonneton, P., Dupuis, H., and Senechal, N.: Double bar beach dynamics on the high-energy meso-macrotidal French Aquitanian coast: a review, *Mar. Geol.*, 245, 141–159, 2007.
- 20 Falqués, A.: Formación de topografía rítmica en el Delta del Ebro, *Revista de Geofísica*, 45, 143–156, 1989.
- Galal, E. M. and Takewaka, S.: Longshore migration of shoreline mega-cusps observed with x-band radar, *Coast. Eng. J.*, 50, 247–276, 2008.
- 25 Garnier, R., Calvete, D., Falqués, A., and Caballeria, M.: Generation and nonlinear evolution of shore-oblique/transverse sand bars, *J. Fluid Mech.*, 567, 327–360, 2006.
- Garnier, R., Calvete, D., Falqués, A., and Dodd, N.: Modelling the formation and the long-term behavior of rip channel systems from the deformation of a longshore bar, *J. Geophys. Res.*, 113, C07053, doi:10.1029/2007JC004632, 2008.

Intertidal finger bars at El Puntal, Bay of Santander, Spain

E. Pellón et al.

Title Page

Abstract

Introduction

Conclusions

References

Tables

Figures

◀

▶

◀

▶

Back

Close

Full Screen / Esc

Printer-friendly Version

Interactive Discussion



Intertidal finger bars at El Puntal, Bay of Santander, Spain

E. Pellón et al.

Title Page

Abstract

Introduction

Conclusions

References

Tables

Figures

◀

▶

◀

▶

Back

Close

Full Screen / Esc

Printer-friendly Version

Interactive Discussion



Garnier, R., Medina, R., Pellón, E., Falqués, A., and Turki, I.: Intertidal finger bars at El Puntal spit, bay of Santander, Spain, Proceedings of the 33rd Conference on Coastal Engineering, ASCE, Santander, Spain, 1–8, 2012.

Gelfenbaum, G. and Brooks, G. R.: The morphology and migration of transverse bars off the west-central Florida coast, *Mar. Geol.*, 200, 273–289, 2003.

Goodfellow, B. W. and Stephenson, W. J.: Beach morphodynamics in a strong-wind bay: a low-energy environment?, *Mar. Geol.*, 214, 101–116, 2005.

Gutiérrez, O., González, M., and Medina, R.: A methodology to study beach morphodynamics based on self-organizing maps and digital images, Proceedings of the Coastal Sediments 2011, World Scientific, 2453–2464, 2011.

Green, M. O., Black, K. P., and Amos, C. L.: Control of estuarine sediment dynamics by interactions between currents and waves at several scales, *Mar. Geol.*, 144, 97–116, 1997.

Holman, R. A., Sallenger Jr., A. H., Lippmann, T. C. D., and Haines, J. W.: The application of video image processing to the study of nearshore processes, *Oceanography*, 6, 78–85, 1993.

Komar, P. and Inman, D.: Longshore sand transport on beaches, *J. Geophys. Res.*, 75, 5514–5527, 1970.

Konicki, K. M. and Holman, R. A.: The statistics and kinematics of transverse sand bars on an open coast, *Mar. Geol.*, 169, 69–101, 2000.

Kroon, A., Davidson, M. A., Aarninkhof, S. G. J., Archetti, R., Armaroli, C., González, M., Medri, S., Osorio, A., Aagaard, T., Holman, R. A., and Spanhoff, R.: Application of remote sensing video systems to coastline management problems, *Coast. Eng.*, 54, 493–505, 2007.

Lafon, V., Dupuis, H., Howa, H., and Froidefond, J. M.: Determining ridge and runnel longshore migration rate using spot imagery, *Oceanol. Acta*, 25, 149–158, 2002.

Levoy, F., Anthony, E. J., Monfort, O., Robin, N., and Bretel, P.: Formation and migration of transverse bars along a tidal sandy coast deduced from multi-temporal Lidar datasets, *Mar. Geol.*, 342, 39–52, 2013.

Longuet-Higgins, M. S. and Stewart, R. W.: Radiation stresses in water waves: a physical discussion with applications, *Deep-Sea Res.*, 11, 529–562, 1964.

Losada, M. A., Medina, R., Vidal, C., and Roldan, A.: Historical evolution and morphological analysis of “El Puntal” Spit, Santander (Spain), *J. Coastal Res.*, 7, 711–722, 1991.

Intertidal finger bars at El Puntal, Bay of Santander, Spain

E. Pellón et al.

Title Page

Abstract

Introduction

Conclusions

References

Tables

Figures

◀

▶

◀

▶

Back

Close

Full Screen / Esc

Printer-friendly Version

Interactive Discussion



Losada, M. A., Medina, R., Vidal, C., and Losada, I. J.: Temporal and spatial cross-shore distributions of sediment at “El Puntal” spit, Santander, Spain, *Coast. Eng.*, 1992, Proceedings of the Twenty-Third International Conference, 2251–2264, 1992.

Medellín, G., Medina, R., Falqués A., and González, M.: Coastline sand waves on a low-energy beach at “El Puntal” spit, Spain, *Mar. Geol.*, 250, 143–156, 2008.

Medellín, G., Falqués A., Medina, R., and González, M.: Coastline sand waves on a low-energy beach at El Puntal spit, Spain: linear stability analysis, *J. Geophys. Res.*, 114, C03022, doi:10.1029/2007JC004426, 2009.

Medina, R., Marino-Tapia, I., Osorio, A., Davidson, M., and Martín F. L.: Management of dynamic navigational channels using video techniques, *Coast. Eng.*, 54, 523–537, 2007.

Menéndez, M., Tomás, A., Camus, P., García-Díez, M., Fita, L., Fernández, J., Méndez, F. J., and Losada, I. J.: A methodology to evaluate regional-scale offshore wind energy resources, OCEANS’11 IEEE Santander Conference, Spain, 1–9, 2011.

Niedoroda, A. W. and Tanner, W. F.: Preliminary study of transverse bars, *Mar. Geol.*, 9, 41–62, 1970.

Nordstrom, K. F. and Jackson, N. L.: Physical processes and landforms on beaches in short fetch environments in estuaries, small lakes and reservoirs: a review, *Earth-Sci. Rev.*, 111, 232–247, 2012.

Price, T. D. and Ruessink, B. G.: State dynamics of a double sandbar system, *Cont. Shelf. Res.*, 31, 659–674, 2011.

Ranasinghe, R., Symonds, G., Black, K., and Holman, R.: Morphodynamics of intermediate beaches: a video imaging and numerical modelling study, *Coast. Eng.*, 51, 629–655, 2004.

Requejo, S., Medina, R., and González, M.: Development of a medium-long term beach evolution model, *Coast. Eng.*, 55, 1074–1088, 2008.

Ribas, F. and Kroon, A.: Characteristics and dynamics of surfzone transverse finger bars, *J. Geophys. Res.*, 112, F03028, doi:10.1029/2006JF000685, 2007.

Ribas, F., Falqués, A., and Montoto, A.: Nearshore oblique sand bars, *J. Geophys. Res.*, 108, C43119, doi:10.1029/2001JC000985, 2003.

Ribas, F., de Swart, H. E., Calvete, D., and Falqués, A.: Modeling and analyzing observed transverse sand bars in the surf zone, *J. Geophys. Res.*, 117, F02013, doi:10.1029/2011JF002158, 2012.

Soulsby, R. L.: *Dynamics of Marine Sands*, Thomas Telford, London, UK, 1997.

Thornton, B. and Guza, R. T.: Transformation of wave height distribution, J. Geophys. Res., 88, 5925–5938, 1983.

Thornton, E. B., MacMahan, J., and Sallenger Jr., A. H.: Rip currents, mega-cusps, and eroding dunes, Mar. Geol., 240, 151–167, 2007.

5 van Enckevort, I. M. J., Ruessink, B. G., Coco, G., Suzuki, K., Turner, I. L., Plant, N. G., and Holman, R. A.: Observations of nearshore crescentic sandbars, J. Geophys. Res., 109, C06028, doi:10.1029/2003JC002214, 2004.

Wijnberg, K. M. and Kroon, A.: Barred beaches, Geomorphology, 48, 103–120, 2002.

10 Wright, L. D., Short, A. D.: Morphodynamic variability of surf zones and beaches: a synthesis, Mar. Geol., 56, 93–118, 1984.

ESURFD

1, 673–710, 2013

Intertidal finger bars at El Puntal, Bay of Santander, Spain

E. Pellón et al.

Title Page

Abstract

Introduction

Conclusions

References

Tables

Figures

◀

▶

◀

▶

Back

Close

Full Screen / Esc

Printer-friendly Version

Interactive Discussion



Intertidal finger bars at El Puntal, Bay of Santander, Spain

E. Pellón et al.

Title Page

Abstract

Introduction

Conclusions

References

Tables

Figures

◀

▶

◀

▶

Back

Close

Full Screen / Esc

Printer-friendly Version

Interactive Discussion



Table 1. Transverse bar types and main characteristics.

Type	Beach type	Mean wave height (m)	Bar wave-length (m)	Cross-shore span (m)	Bar orientation	Migration speed ^a (mday ⁻¹)	Reference of observed bars
TBR (Transverse Bars and Rips)	Intermediate wave-dominated beaches	> 0.5	100–500	< 150	Normal, Oblique	5 ^b	Wright and Short (1984) Lafon et al. (2002) Ranasinghe et al. (2004) Goodfellow and Stephenson (2005) ^c Castelle et al. (2007) Thornton et al. (2007)
Large Scale Finger Bars	Low energy beaches, wide (~ 1 km) with gentle slope (0.002)	< 0.5	~ 100	~ 1000	Normal or slightly oblique	1	Niederoda and Tanner (1970) Gelfenbaum and Brooks (2003) Levoy et al. (2013)
Finger Bars of Intermediate Beaches	Intermediate wave-dominated beaches	> 0.5	50–100	< 100	Oblique up-current oriented	40	Konicki and Holman (2000) Ribas and Kroon (2007)
Small Scale Finger Bars	Very fetch – limited (< 10 km)	< 0.1	< 50	< 100	Oblique down-current oriented	Lack of data	Falqués (1989) Bruner and Smosna (1989) Nordstrom and Jackson (2012) Garnier et al. (2012) Present study

^a The values given for the migration speed are the maximum alongshore velocities detected.

^b Some studies have detected alongshore migration speed of crescentic bars (van Enckevort et al., 2004) and of mega-cusps (Galal and Takewaka, 2008) much larger (~ 50 m day⁻¹) but these systems are not clearly coupled with TBR.

^c Identify smaller scale TBR in low energy environment.

Intertidal finger bars at El Puntal, Bay of Santander, Spain

E. Pellón et al.

Title Page

Abstract

Introduction

Conclusions

References

Tables

Figures

◀

▶

◀

▶

Back

Close

Full Screen / Esc

Printer-friendly Version

Interactive Discussion



Table 2. Result of the correlation.

Sediment Transport	Without Tidal Coefficient	With Tidal Coefficient
Constant stirring, wind-waves alone	0.46	0.44
Constant stirring, wind alone	0.49	0.45
Constant stirring, total velocity	0.49	0.45
Soulsby and Van Rijn Formula	0.58	0.60

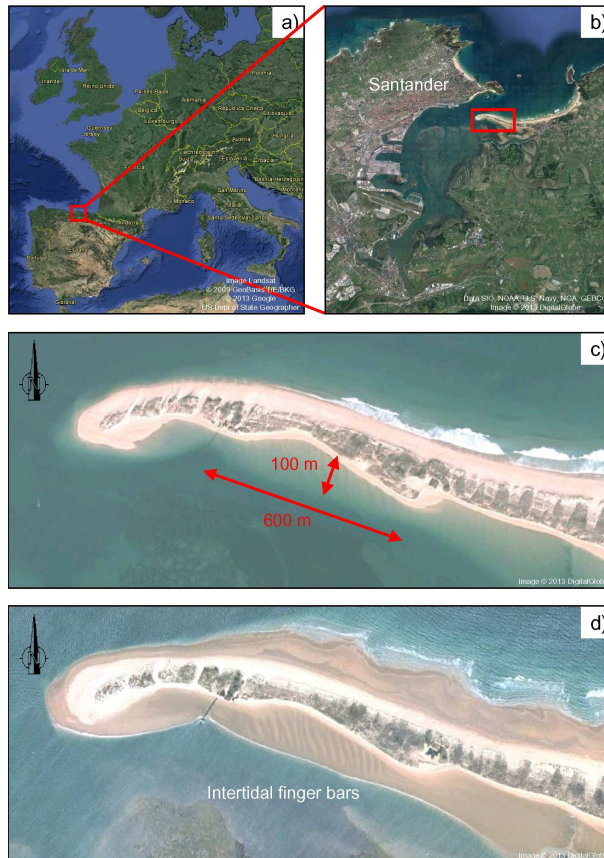


Fig. 1. (a) Location of Santander, (b) Map of the bay, (c) El Puntal at high tide, (d) El Puntal at low tide. Images from Google Earth.

Intertidal finger bars at El Puntal, Bay of Santander, Spain

E. Pellón et al.

Title Page

Abstract

Introduction

Conclusions

References

Tables

Figures



Back

Close

Full Screen / Esc

Printer-friendly Version

Interactive Discussion



**Intertidal finger bars
at El Puntal, Bay of
Santander, Spain**

E. Pellón et al.



Fig. 2. Photos at **(a, b)** low tide, **(c, d)** rising tide. Pictures taken from the east end of the study area **(a, c)**, and from the west end **(b, d)**. Capture date: 25 February 2012.

Title Page

Abstract

Introduction

Conclusions

References

Tables

Figures

◀

▶

◀

▶

Back

Close

Full Screen / Esc

Printer-friendly Version

Interactive Discussion



**Intertidal finger bars
at El Puntal, Bay of
Santander, Spain**

E. Pellón et al.

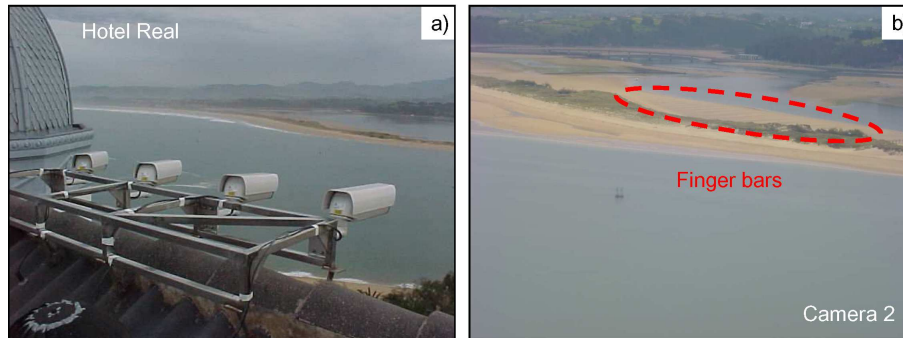


Fig. 3. Horus video system. **(a)** Cameras at the roof of the Hotel Real, **(b)** Image taken by camera 2.

Title Page

Abstract

Introduction

Conclusions

References

Tables

Figures

◀

▶

◀

▶

Back

Close

Full Screen / Esc

Printer-friendly Version

Interactive Discussion



Intertidal finger bars at El Puntal, Bay of Santander, Spain

E. Pellón et al.

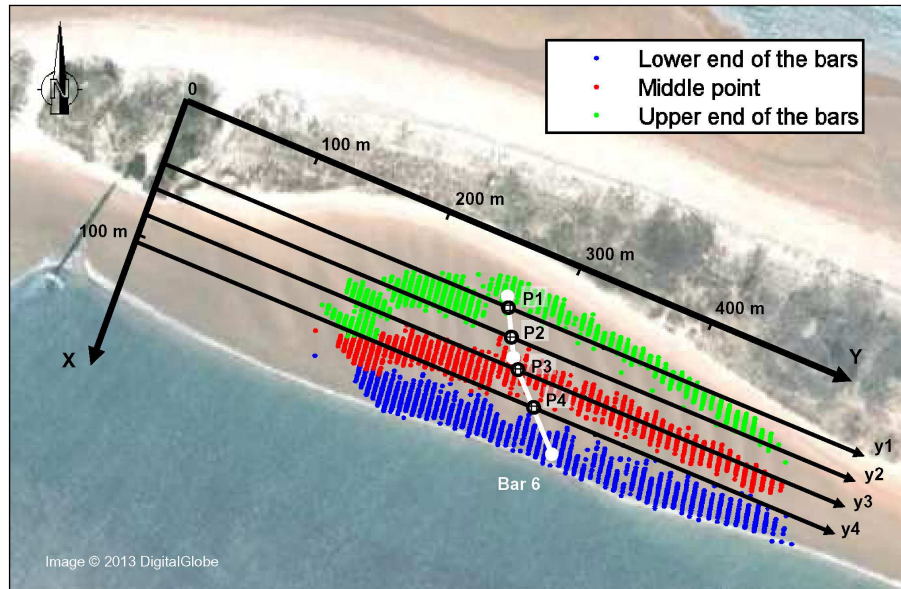


Fig. 4. Coordinate system and bar digitization. The x and y axes stand for the cross-shore and the alongshore direction, respectively. The color points represent the digitized data (each bar is represented by 3 points); blue, red and green are the outer, the middle and the inner points of the bars, respectively. The bar positions (P1–P4) are defined along the y_1 – y_4 axes (see positions of Bar 6, in white).

Title Page

Abstract

Introduction

Conclusions

References

Tables

Figures

◀

▶

◀

▶

Back

Close

Full Screen / Esc

Printer-friendly Version

Interactive Discussion



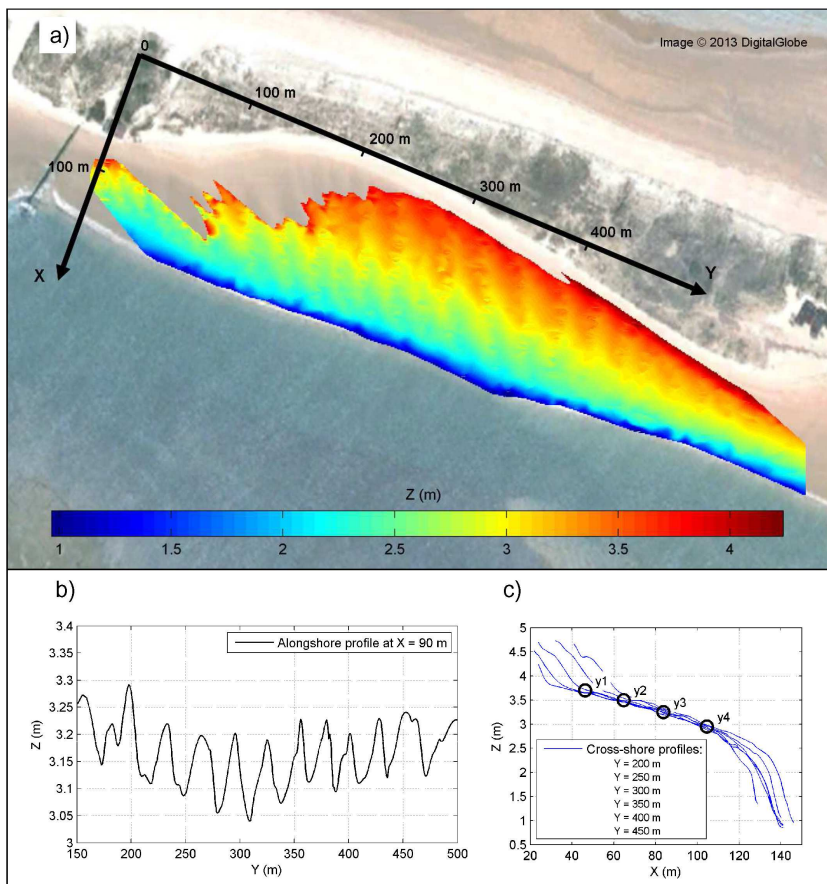


Fig. 5. (a) Bathymetry reconstruction (24 June 2008). The north-west area without data is the shadowed area by the dune, from the point of view of the camera. (b) Alongshore profile of the bed level. (c) Cross-shore profiles of the bed level and cross-shore positions of the y_1 – y_4 axes.

**Intertidal finger bars
at El Puntal, Bay of
Santander, Spain**

E. Pellón et al.

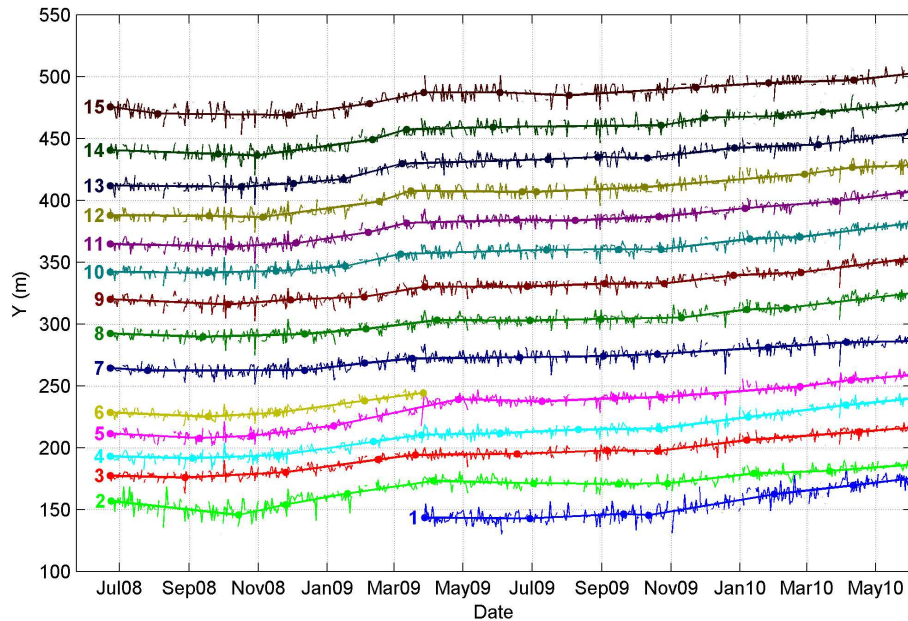


Fig. 6. Evolution of the bar system. Time series of the bar position along the y_3 axis. The thin discontinuous lines represent the measured position. The thick segments represent the piecewise regression of the measured position. The number at the left side of each lines indicates the bar number.

Title Page

Abstract

Introduction

Conclusions

References

Tables

Figures

◀

▶

◀

▶

Back

Close

Full Screen / Esc

Printer-friendly Version

Interactive Discussion



Intertidal finger bars at El Puntal, Bay of Santander, Spain

E. Pellón et al.

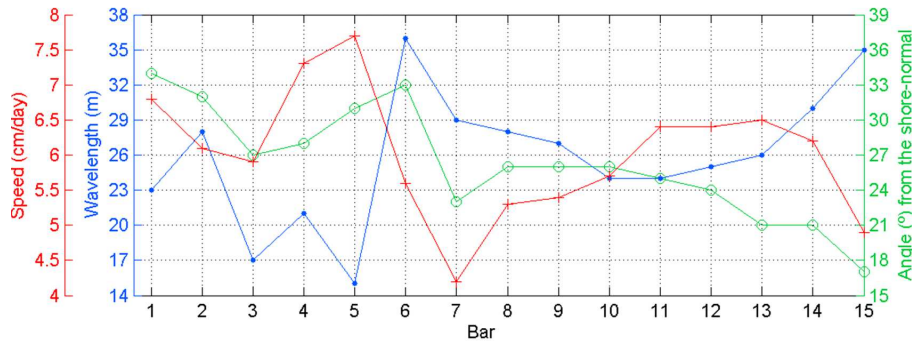


Fig. 7. Mean wavelength, angle and speed (averaged on time) of each bar. The bar angles are measured from the shore-normal to the east. Positive values of the bar speeds represent movements of the bars to the east.

Title Page

Abstract

Introduction

Conclusions

References

Tables

Figures

◀

▶

◀

▶

Back

Close

Full Screen / Esc

Printer-friendly Version

Interactive Discussion



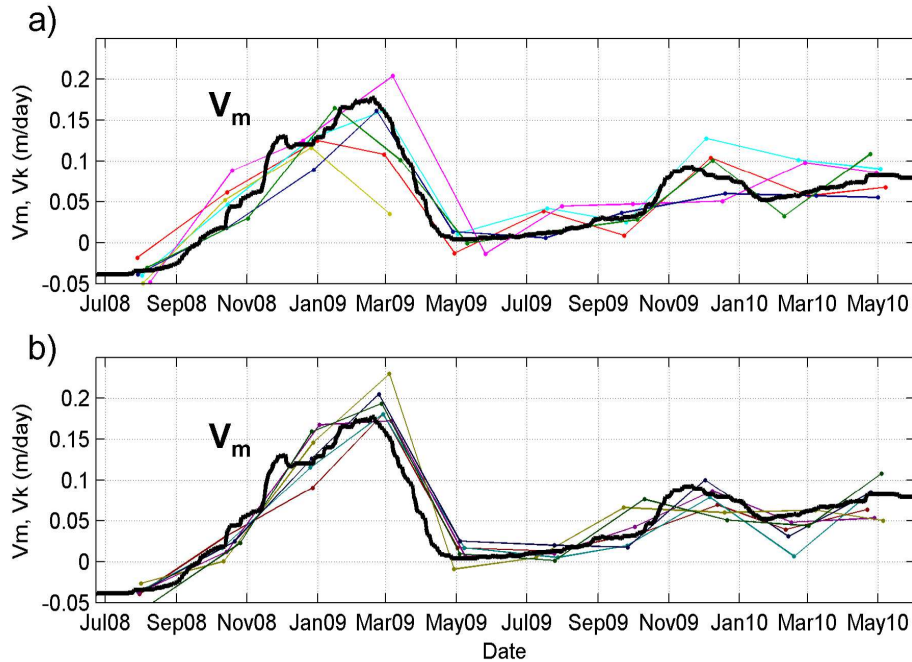


Fig. 8. Migration speed of the transverse bars. V_m (thick-black line), migration velocity of the bar system. V_k (color lines), individual bar migration velocity (the colors correspond to Fig. 6). **(a)** V_k for bars 3–8. **(b)** V_k for bars 9–11.

Title Page

Abstract

Introduction

Conclusions

References

Tables

Figures

◀

▶

◀

▶

Back

Close

Full Screen / Esc

Printer-friendly Version

Interactive Discussion



Intertidal finger bars at El Puntal, Bay of Santander, Spain

E. Pellón et al.

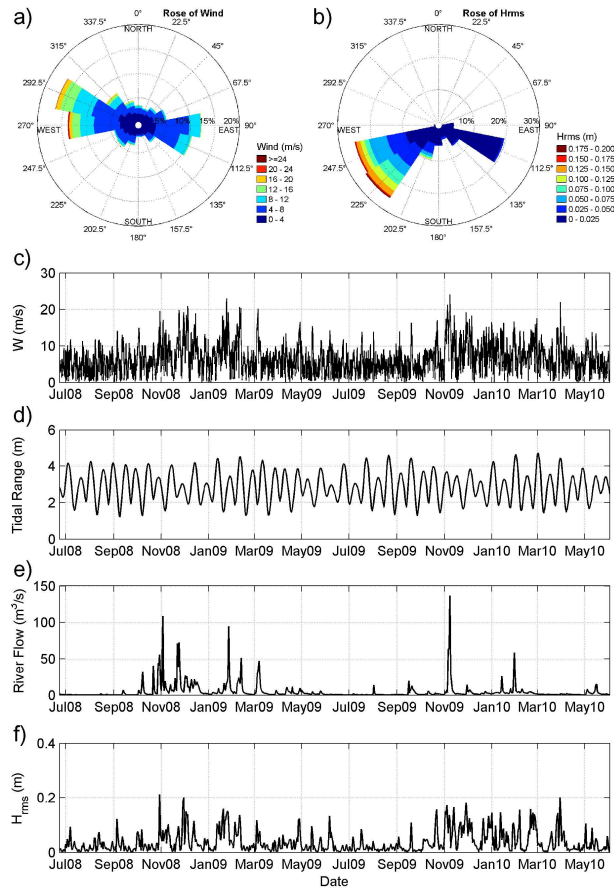


Fig. 9. (a) Wind rose. (b) Wave rose. (c–f) Time series of the (c) wind speed W , and the daily averaged (d) tidal range, (e) river flow rate, (f) root-mean-square wave height of the wind waves H_{rms} .

Intertidal finger bars at El Puntal, Bay of Santander, Spain

E. Pellón et al.

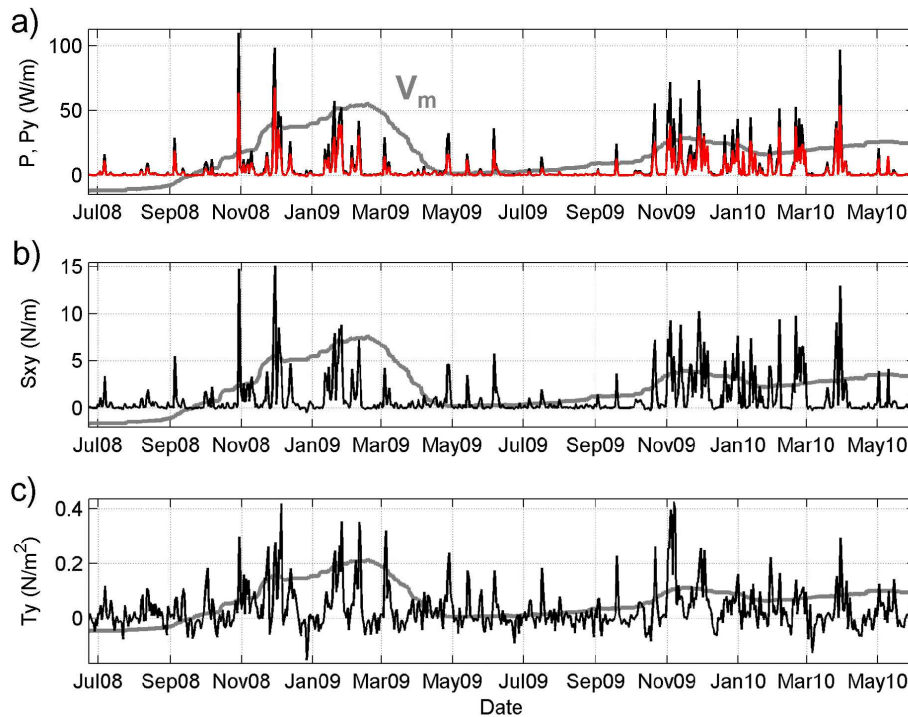


Fig. 10. Time series of the daily averaged **(a)** wave power (P , black) and alongshore wave power (P_y , red), **(b)** alongshore component of the wave radiation stress (S_{xy} , black), and **(c)** alongshore wind stress (T_y , black). The gray lines represent the behaviour of the bar migration velocity V_m that has been redimensionalized with the above variables.

Title Page

Abstract

Introduction

Conclusions

References

Tables

Figures

◀

▶

◀

▶

Back

Close

Full Screen / Esc

Printer-friendly Version

Interactive Discussion



Intertidal finger bars at El Puntal, Bay of Santander, Spain

E. Pellón et al.

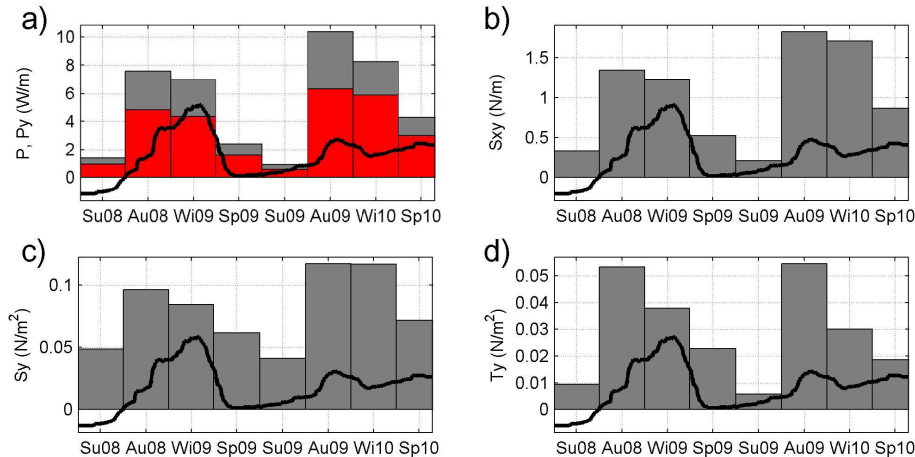


Fig. 11. Seasonal variability of **(a)** wave power (P , gray) and alongshore wave power (P_y , red), **(b)** alongshore component of the wave radiation stress (S_{xy}), **(c)** alongshore wave stress (S_y), and **(d)** alongshore wind stress (T_y). The black lines represent the behaviour of the bar migration velocity V_m that has been redimensionalized with the above variables. The bottom axes indicate the seasons, from summer 2008 to spring 2010.

Intertidal finger bars at El Puntal, Bay of Santander, Spain

E. Pellón et al.

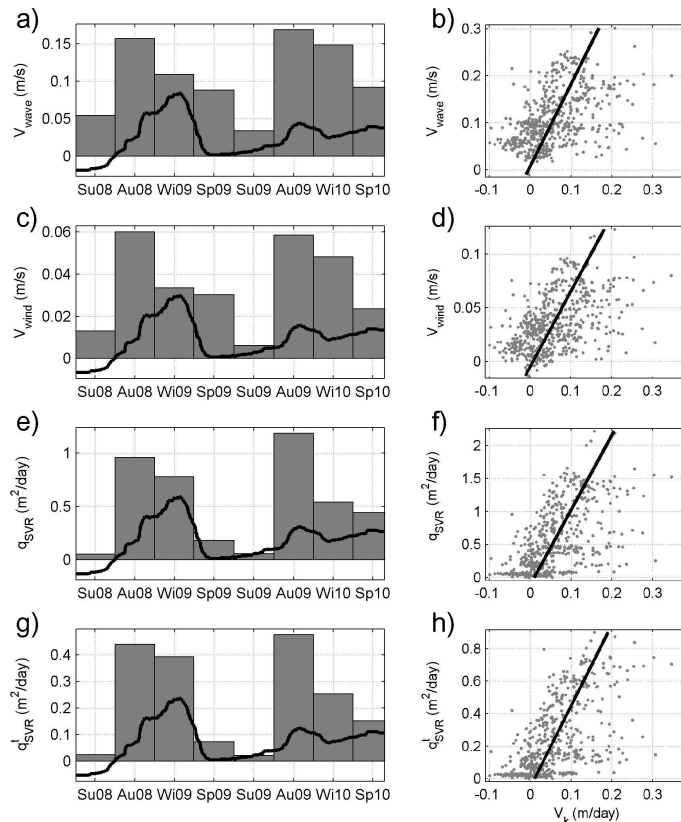


Fig. 12. Sediment transport evaluation. Analysis of (from top to bottom): **(a, b)** alongshore current driven by the wind-waves (V_{wave}), **(c, d)** alongshore current driven by the wind (V_{wind}), **(e, f)** alongshore component of the Soulsby and Van Rijn (SVR) formula (q_{SVR}), and **(g, h)** SVR formula with tidal correction (q_{SVR}^t). Left **(a, c, e, g)**: seasonal variability (see caption of Fig. 11). Right **(b, d, f, h)**: scatter plot and linear regression between the above variables and the bar migration velocity (V_k).